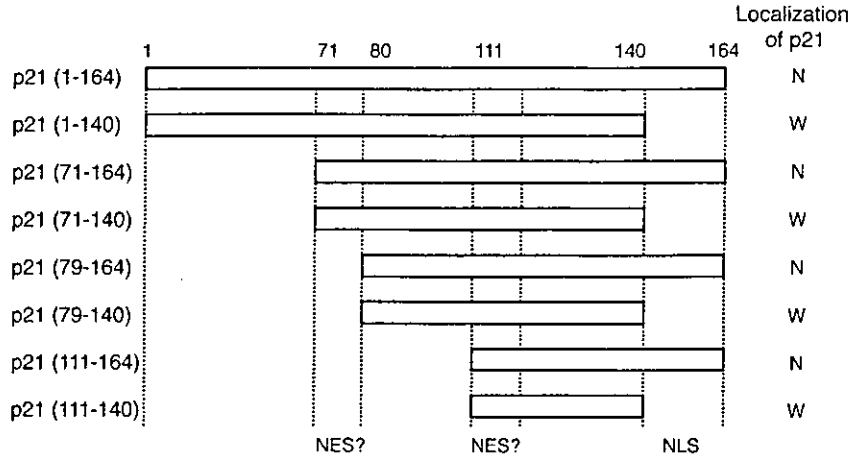

FIG. 1. Subcellular localization of p21 is determined by its nuclear localization signal. Predicted nuclear export-like signals are located at aa 71 to 79 and 111 to 119. NLS is located at aa 141 to 164. Fragments from p21 depicted were C terminally fused with GFP in pEGFP plasmids. These vectors were introduced into HeLa cells, and the subcellular localization of GFP signals was determined. N, nucleus; W, whole-cell compartment.

anoside to a final concentration of 0.4 mM in an exponentially growing bacterial culture at 30°C.

Cell culture and transfection. HeLa and HEK293 cells were cultured in minimum essential medium (Sigma) with 10% fetal bovine serum in 5% CO_2 humidified atmosphere at 37°C. WEHI3B D+, HL60, and U937 cells were cultured in RPMI 1640 (GIBCO/BRL) with 10% fetal bovine serum in 5% CO_2 humidified atmosphere at 37°C. HeLa and HEK293 cells were transfected by using Effectene (QIAGEN). WEHI3B D+ and U937 cells were transfected by electroporation.

In vitro differentiation of WEHI3B D+, HL60, and U937 cells. Twenty-four hours after electroporation of WEHI3B D+ cells, medium was replaced with 1 mg of G418-containing medium/ml. Cells were seeded into 96-well plates. GFP signals were checked by fluorescence microscopy, and GFP-positive wells were maintained and expanded. Several wells with GFP-positive cells were selected, and cells were transferred to glass-bottomed culture dishes, to which tetradecanoyl phorbol acetate (TPA) and VD_3 were then added at final concentrations of 50 ng/ml and 50 nM, respectively. Cells were then examined by confocal microscopy.

HL60 and U937 cells were induced to differentiate in the presence of 50 nM VD_3. U937/CB6-p21 cells were induced to differentiate after the addition of zinc to the culture medium, as reported previously (2).

Confocal microscopy. Nuclei were visualized by the addition of Hoechst 33258. Fluorescence images were recorded by a confocal laser-scanning microscope (LSM-GB200; Olympus).

Brap2 mRNA expression analysis. Brap2 mRNA expression was analyzed by reverse transcriptase (RT)-PCR using the following primers: Brap2 5′ primer, 5′-ATGAGTGTGTCACTGGTTGTTATCC-3′; Brap2 3′ primer, 5′-TCAGGG ATGTCTGTTGCTCTGA-3′.

In vitro binding assay. Myc-tagged Brap2 was translated in vitro from the pBluescript-KS vector using a TNT-coupled transcription-translation system (Promega) in the presence of [^{35}S]methionine (Dai-ichi Pharmaceuticals Inc.). Glutathione-Sepharose beads containing about 20 μg of GST or GST fusion proteins were preincubated with Tris-buffered saline buffer (25 mM Tris-HCl [pH 8.0], 120 mM NaCl, 10% bovine serum albumin) also containing protease inhibitors for 30 min at room temperature with rotation. The beads were then incubated with translated in vitro products in standard lysis buffer (100 mM NaCl, 50 mM Tris [pH 7.4], 5 mM EDTA, 0.5% Triton X-100, and protease inhibitors) for 1 h at room temperature with rotation. Complexes were washed extensively with standard lysis buffer, boiled in protein loading buffer, separated by sodium dodecyl sulfate-polyacrylamide gel electrophoresis (SDS-PAGE), and detected with image analyzer Bas 2000 (Fuji-Xerox).

Antibody preparation. The cDNA sequence of Brap2 corresponding to aa 423 to 570, amplified by PCR from RNA derived from differentiated U937 cells, was cloned in frame with a six-His tag sequence in the expression vector pTrc-His-B (Invitrogen). After transformation with the resulting pTrc-His-Brap2-C plasmid and 6 h of induction with 100 mM isopropyl-β-D-thiogalactopyranoside), bacteria were lysed in 6 M urea, sonicated, and centrifuged, and the recombinant protein was purified from the supernatant by Ni-nitrilotriacetic acid agarose (Amersham-Pharmacia) and 100 to 500 mM imidazole elution. Sera from rabbits immunized with the recombinant protein were affinity purified.

Western blotting and immunoprecipitation. Cell lysates were prepared in a lysis buffer (150 mM NaCl, 1% Nonidet P-40, 0.1% SDS, 1% sodium deoxycholate, 5 mM EDTA, 10 mM Tris [pH 7.4]) containing protease inhibitors. Proteins were separated by SDS-PAGE and transferred to polyvinylidene difluoride membranes (Millipore). Western blotting was performed with the following primary antibodies: anti-GFP polyclonal antibody (PAb) (Living Colors; Clontech), anti-p21 monoclonal antibody (MAb) (C24420; Transduction Laboratories), anti-Myc PAb (MBL), and anti-Flag MAb (M2; Sigma). Binding of the primary antibody was detected by using a commercial ECL kit (Amersham-Pharmacia). Immune complexes were immunoprecipitated from clarified cell lysates with mouse immunoglobulin G (IgG) M280 magnetic beads (Dynal) preincubated with antibody to p21. The beads were washed extensively with washing buffer (150 mM NaCl, 10 mM Tris [pH 7.4], 0.5% Triton X-100, 5 mM EDTA), boiled in loading buffer, separated by SDS-PAGE, and subjected to Western blot analysis.

RNA interference. Double-stranded RNAs were produced by in vitro transcription using the Silencer siRNA construction kit (Ambion) according to the manufacturer's instructions. We prepared siRNA targeting human Brap2; the target sequence was 5′-AACCAATATATGGTGCTGATA-3′. The control siRNA sequence was 5′-AACCAATGGTATATGCTGATA-3′. U937 cells were transfected with 400 pmol of double-stranded siRNA using GenomOne HVJ envelope vector kit (Ishihara Sangyo Kaisha) according to the manufacturer's instructions.

Fluorescence-activated cell sorter analysis. Aliquots of cells were stained with fluorescein isothiocyanate-conjugated anti-CD14 (Nichirei). For the cell survival assay, aliquots of cells were stained with rhodamine 123 and merocyanine 540 (Molecular Probes). Cells that showed a low level of staining with rhodamine 123 and a high level of staining with merocyanine 540 were counted for dead cells. The analysis was performed with a FACSCalibur cytometer (Becton Dickinson).

RESULTS

Localization of p21 is determined by NLS. p21 contains several functional regions, including cyclin-binding domain 1 (aa 21 to 26), cyclin-binding domain 2 (aa 153 to 159), Cdk-binding domain (aa 49 to 71), PCNA-binding domain (aa 141 to 160), and NLS (aa 140 to 159). We also found that p21 carries NES-like sequences (aa 71 to 79 and 111 to 120). We constructed several GFP-p21 deletion mutant-fusion vectors as depicted in Fig. 1. The introduction of these expression vectors into HeLa cells revealed that p21 localized exclusively to the

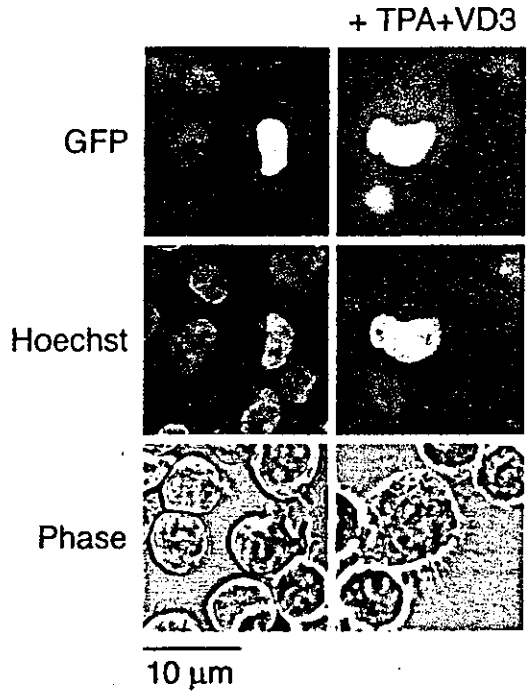

FIG. 2. Cytoplasmic expression of p21 depends on NLS in monocytic differentiation. GFP signals in cells transfected with GFP-tagged p21-NLS constructs are shown. WEHI3B D+ cells were transfected with a construct containing GFP fused with p21 (aa 80 to 164). GFP-positive cells were selected and cultured with 50 ng of TPA/ml and 50 nM VD_3 and then examined by confocal microscopy. Photos in the left and right columns show transfected cells before and after culture with TPA plus VD_3, respectively. Monocytic differentiation induction resulted in the cytoplasmic expression of GFP signal in cells transfected with p21-NLS. TPA plus VD_3 induced no difference of GFP signal in cells transfected with the p21 construct without NLS. Top, middle, and bottom panels show GFP signals, nuclear staining with Hoechst 33258, and a phase-contrast view of the corresponding fields, respectively.

nucleus in the presence of NLS. In the absence of NLS, GFP signals were detected in all cell compartments.

Because changes in the subcellular localization of p21 were observed in a monocyte differentiation system, we took advantage of the murine promonocytic cell line WEHI3B D+, which has been demonstrated to differentiate to monocytic cells associated with characteristic morphological change in the presence of TPA plus VD_3 (4). These cells were treated with TPA plus VD_3 to determine the effect of differentiation on the behavior of the GFP-p21 fusion proteins. To this end, the GFP-p21 fusion vectors depicted in Fig. 1 were electroporated into WEHI3B D+ cells, and after incubation with TPA, the subcellular localization of GFP signals was analyzed by confocal microscopy. In the presence of NLS, GFP signals were seen exclusively in the nucleus before treatment with TPA plus VD_3. However, after treatment with TPA plus VD_3, GFP signals appeared in the cytoplasm associated with the morphological change of WEHI3B D+ (Fig. 2, top panel). These results suggest that the negative regulation of NLS is involved in the determination of the subcellular location of p21 during monocytic differentiation. In the absence of NLS, GFP signals were detected in both the nucleus and the cytoplasm. TPA plus VD_3 induced no significant difference in GFP signals in cells transfected with the constructs without NLS.

Brap2 binds to NLS of p21 and functions as a cytoplasmic retention protein. We could not detect any mobility shift of p21 protein in SDS-PAGE and subsequent Western blot analyses before or after monocytic differentiation of U937 cells. This result renders modifications of p21, such as phosphorylation, unlikely.

Brap2 is a unique cytoplasmic protein isolated as the NLS-interacting protein of BRCA1 (13) (data not shown). Brap2 has been characterized as binding to several NLSs, including bipartite types. We therefore assessed whether Brap2 interacts with p21 protein by using an in vitro GST pull-down assay. An in vitro-translated full-length Brap2 carrying a c-Myc epitope was incubated with GST alone, GST-p21-dNLS-C (aa 87 to 140), GST-p21-C (aa 87 to 164), or GST-p21 (aa 2 to 164). As shown in Fig. 3A, Brap2 binds to GST-p21-C and GST-p21 but not to GST alone or GST-p21-dNLS-C. These results suggest that Brap2 directly binds p21 through its NLS motif. To further confirm this interaction in vivo, cotransfection immunoprecipitation experiments were done using HEK293 cells. GFP-Brap2 vectors were cotransfected with C-terminally Myc-tagged p21 (aa 1 to 164) or Flag-tagged dNLS-p21 (aa 1 to 140). As shown in Fig. 3B and C, Brap2 binds full-length p21 but not dNLS-p21. HEK293 cells express a C-terminal truncated form of p21 (17), which no longer interacts with Brap2 (Fig. 3C and data not shown). These results support our finding that Brap2 binds to p21 through NLS.

We then tested the hypothesis that p21 NLS function could be blocked by interaction with Brap2. GFP signals were found exclusively in the nucleus when the GFP-p21-NLS (aa 80 to 164) expression vector was transfected with a mock vector, pCMV-Tag1, into HeLa cells. In contrast, a GFP signal was detected in cytoplasm when the GFP-p21-NLS vector was cotransfected with the Brap2 expression vector, pCMV-Tag1/Brap2 (Fig. 4). Total GFP-positive cells made up about 20% and 10% of the cells in cotransfectants with mock vector and Brap2, respectively. About 20% of GFP-positive cells showed cytoplasmic GFP signals in the cotransfectants with pCMV-Tag1/Brap2, while only about 5% showed weak cytoplasmic GFP signals in the cotransfectants with mock vector.

C-terminal site of Brap2 binds to NLS of p21. Next we mapped the p21 binding site on Brap2. The latter possesses C_2H_2 zinc fingers in the middle and leucine heptad repeats in the C terminus. Three truncation mutants of Brap2, designated Brap2-N (aa 2 to 187) and Brap2-M (aa 168 to 420), which include zinc fingers, and Brap2-C (aa 406 to 600), which includes leucine heptad repeats, were expressed as GFP-tagged fusions. Subcellular localization of GFP signals with Brap2-N and Brap2-M were detected in the whole-cell compartment, but Brap2-C was detected exclusively in cytoplasm (data not shown). These vectors together with Myc-tagged p21 were transfected into HEK293 cells, and their associations were analyzed with a coimmunoprecipitation assay. Only the C-terminal domain of Brap2 was able to bind to p21 (Fig. 5).

Upregulation of Brap2 expression during monocytic differentiation. When we examined the expression of Brap2 in U937 and HL60 cells, we found a modest increase (about 1.5- and 2-fold, respectively) of mRNA levels following VD_3 treatment for 3 days. At this stage, 58% of U937 cells and 62% of HL60

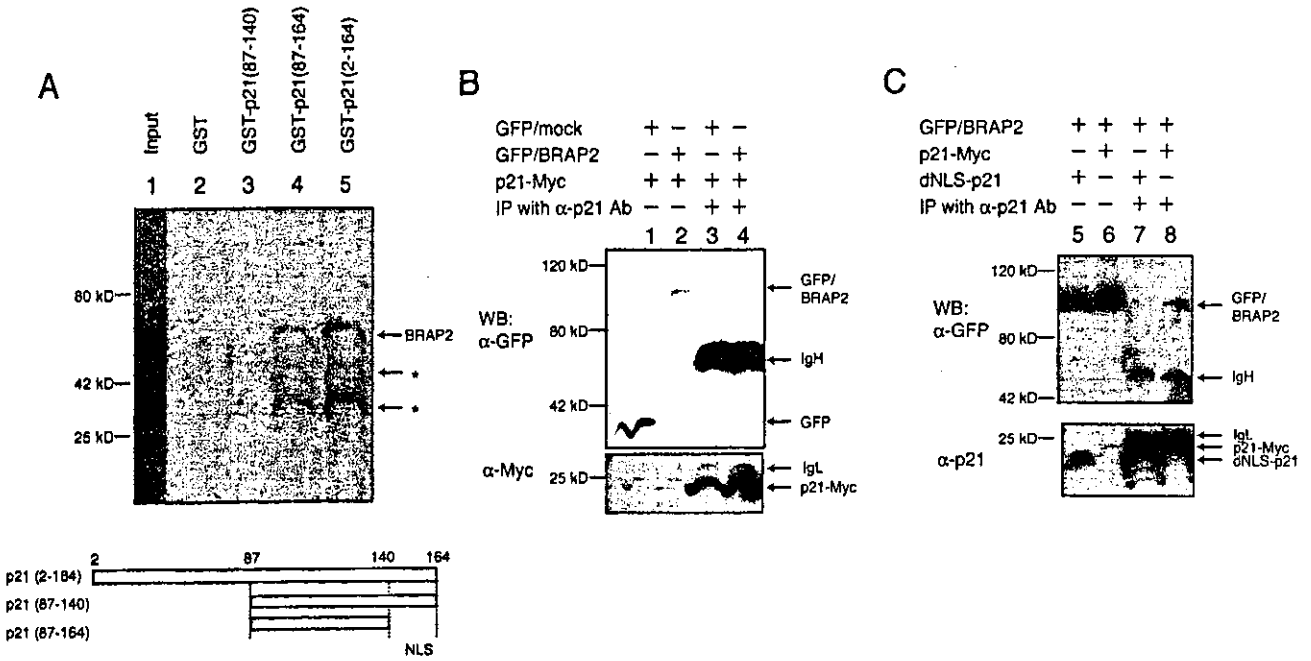

FIG. 3. Brap2 interacts with p21 in vitro and in vivo. (A) Brap2 was translated in vitro in the presence of [^{35}S]methionine and was incubated with glutathione agarose coated with GST alone (lane 2), GST-p21 (aa 87 to 140) (lane 3), GST-p21 (aa 87 to 164) (lane 4), or GST-p21 (aa 2 to 164) (lane 5). Boiled beads were electrophoresed. The input product is shown in lane 1. The top band (about 60 kDa) represents Brap2. Asterisks indicate degradation products of Brap2. (B and C) HEK293 cells were transiently cotransfected with pEGFP-Brap2 and pCMV-p21-Myc vectors (lanes 2, 4, 6, and 8), cotransfected with pEGFP and pCMV-p21-Myc (lanes 1 and 3), or cotransfected with pEGFP-Brap2 and pCMV-dNLS-p21 (lanes 5 and 7). Cell lysate from each sample was immunoprecipitated (IP) with anti-p21 MAb. WB, Western blotted with. (B) p21 interacts with GFP-tagged Brap2 but not GFP alone. The expression of GFP-fused Brap2 in whole lysates (lanes 1 and 2) and p21 immune complexes (lanes 3 and 4) is demonstrated by anti-GFP PAb (upper panel). The expression of C-terminally Myc-fused p21 in whole lysates (lanes 1 and 2) and p21 immune complexes (lanes 3 and 4) is demonstrated by anti-Myc PAb (lower panel). The heavy and light chains of the precipitating antibody (IgH and IgL, respectively) are indicated. (C) Brap2 interacts with NLS of p21. The expression of GFP-fused Brap2 in whole lysates (lanes 5 and 6) and p21 immune complexes (lanes 7 and 8) is demonstrated by anti-GFP PAb (upper panel). The expression of p21 and dNLS-p21 in whole lysate (lanes 5 and 6) and p21 immune complexes (lanes 7 and 8) is demonstrated by anti-p21 MAb (lower panel). The heavy and light chains of the precipitating antibody (IgH and IgL) are indicated.

cells were CD14 positive. Under the same conditions, p21 mRNA levels significantly increased (2, 10, 22) (Fig. 6).

To examine the expression of Brap2 at the protein level, we raised an antibody against the C-terminal region (aa 423 to 570) of human Brap2, which recognizes full-length Brap2 and Brap2-C but not Brap2-N or Brap2-M (Fig. 7A). To assess differentiation-associated expression of Brap2, U937/CB6-p21 and U937/CB6-mock cells were treated with zinc. In this system, the addition of zinc leads to p21 expression, and zinc treatment for 3 days induces monocyte differentiation only in U937/CB6-p21 cells (2). As shown by immunocytochemical staining, zinc treatment induced Brap2 expression only in U937/CB6-p21 but not U937/CB6 cells with mock protein (U937/CB6-mock) (Fig. 7B; data not shown for U937/CB6-mock). U937/CB6-p21 cells treated with zinc for 3 days showed significant induction of Brap2 expression and differentiation (Fig. 7C). Furthermore, induced Brap2 was coimmunoprecipitated with induced p21 (Fig. 7D).

siRNA against Brap2 does not inhibit differentiation but inhibits apoptosis resistance. To address the significance of Brap2 expression for cytoplasmic p21 localization, we set up small interfering RNAs (siRNAs) targeting Brap2 (9). Brap2-targeting siRNA but not control siRNA significantly reduced GFP-Brap2 expression without any reduction of control GFP expression (unpublished data). U937/CB6-p21 cells were transfected with an siRNA targeting Brap2 or control siRNA, and then p21 expression was induced by zinc. After 3 days of incubation with Zn, we analyzed monocytic differentiation by examining CD14 expression, p21 subcellular localization, and cell viability after hydrogen peroxide treatment. Cells treated with any siRNAs showed no significant change in CD14 expression. Brap2-targeting siRNA-treated cells showed considerable reduction of cytoplasmic p21 expression compared to control siRNA-treated cells concomitantly with decreased apoptosis resistance to hydrogen peroxide (Fig. 8).

DISCUSSION

The NLS and NES system is one of the major mechanisms for active transport of molecules into and/or out of the nucleus. This system is regulated by shuttling carriers, such as importin and exportin complexes in cooperation with the Ran-GTP and GTP hydrolysis system (11). Subcellular localization of proteins is determined not only by identifying the presence of NLS or NES sequences but also by altering the accessibility of these regions, for example, as a result of cell signaling. NF-κB NLS is masked by interaction with IκB, which is degraded by IκB kinase activated by proinflammatory cytokines. NF-AT resides

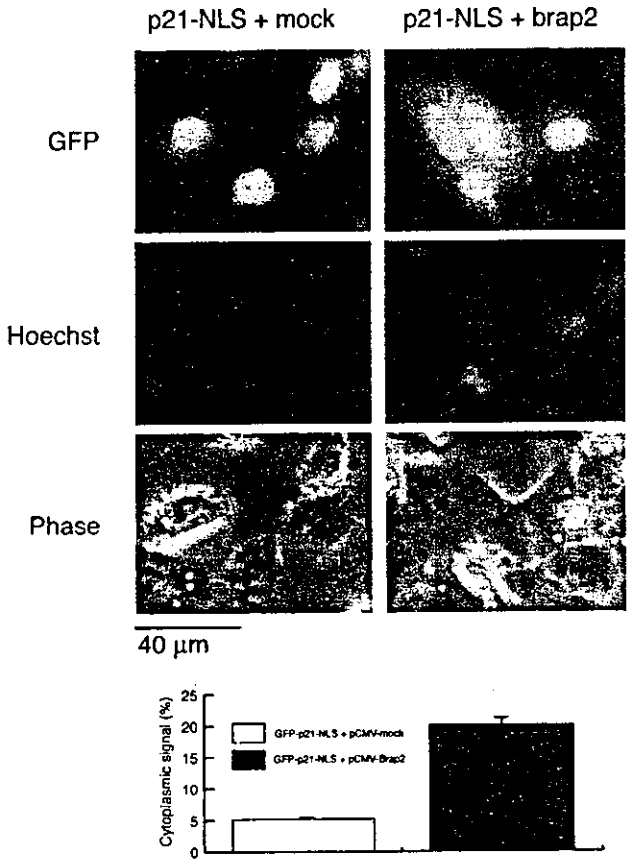

FIG. 4. Brap2 retains p21 in cytoplasm. HeLa cells were cotransfected with GFP-p21-NLS vector with mock or Brap2 vector. GFP signals were detected by fluorescence microscopy. Photographs in the left columns show cells transfected with mock vector, and those in the right columns show cells transfected with Brap2. Top panels show GFP signals, middle panels show DNA stained with Hoechst 33258, and bottom panels show a phase-contrast view of the corresponding fields. The bar graph shows the mean percentage of cells with GFP signals in the cytoplasm ± standard deviation.

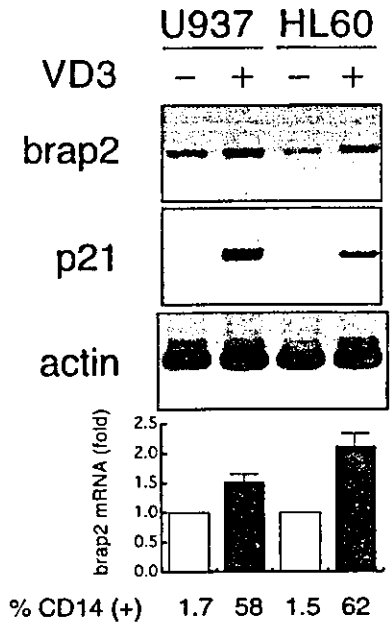

FIG. 6. Expression of Brap2 mRNA is increased during monocytic differentiation of U937 cells. Brap2 expression was analyzed by RT-PCR before and after monocytic differentiation induction of U937 cells (top gel). RNA was extracted from U937 or HL60 cells cultured with or without VD_3 for 3 days. p21 expression was induced by VD_3 in U937 and HL60 cells, as demonstrated by RT-PCR (middle gel). Actin mRNA was amplified by RT-PCR and shown as an internal control (bottom gel). The bar graph shows the increase (n-fold) of VD_3-induced Brap2 transcript standardized to samples without VD_3 treatment. The percentage of cells that were CD14 positive is shown below the bars.

in the cytoplasm in unstimulated T lymphocytes. NF-AT NLS in resting T cells is dephosphorylated in response to stimulation, and this causes its nuclear translocation (8). Similar phosphorylation- or dephosphorylation-dependent modification of NLS and NES are involved in modifications of cyclin B and cyclin D during cell cycle progression (1, 24). Thus, the sub-

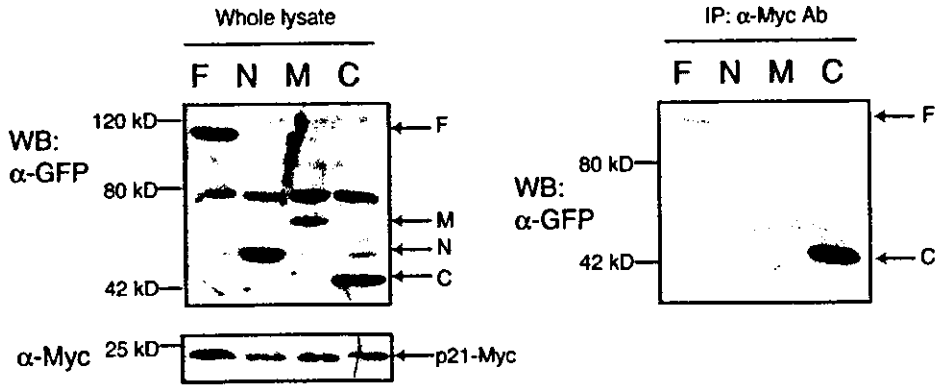

FIG. 5. p21 interaction domain on Brap2. pEGFP vectors containing each of the deletion mutant constructs of Brap2, including Brap2 (F; aa 2 to 600), Brap2-N (N; aa 2 to 187), Brap2-M (M; aa 168 to 420), and Brap2-C (C; aa 406 to 600) were transiently cotransfected with pCMV-p21-Myc into HEK293 cells. Cell lysates from each sample were immunoprecipitated (IP) by anti-Myc PAb. The left panel shows the expression of each of the GFP-fused Brap2 deletion mutants demonstrated by anti-GFP PAb (upper panel) and the expression of p21-Myc by anti-Myc PAb (lower panel) in whole lysate. The right panel shows the interaction of Myc-tagged p21 and the deletion mutant of Brap2 in cells. The immune complex of Myc-tagged p21 was analyzed by Western blotting (WB) with anti-GFP PAb.

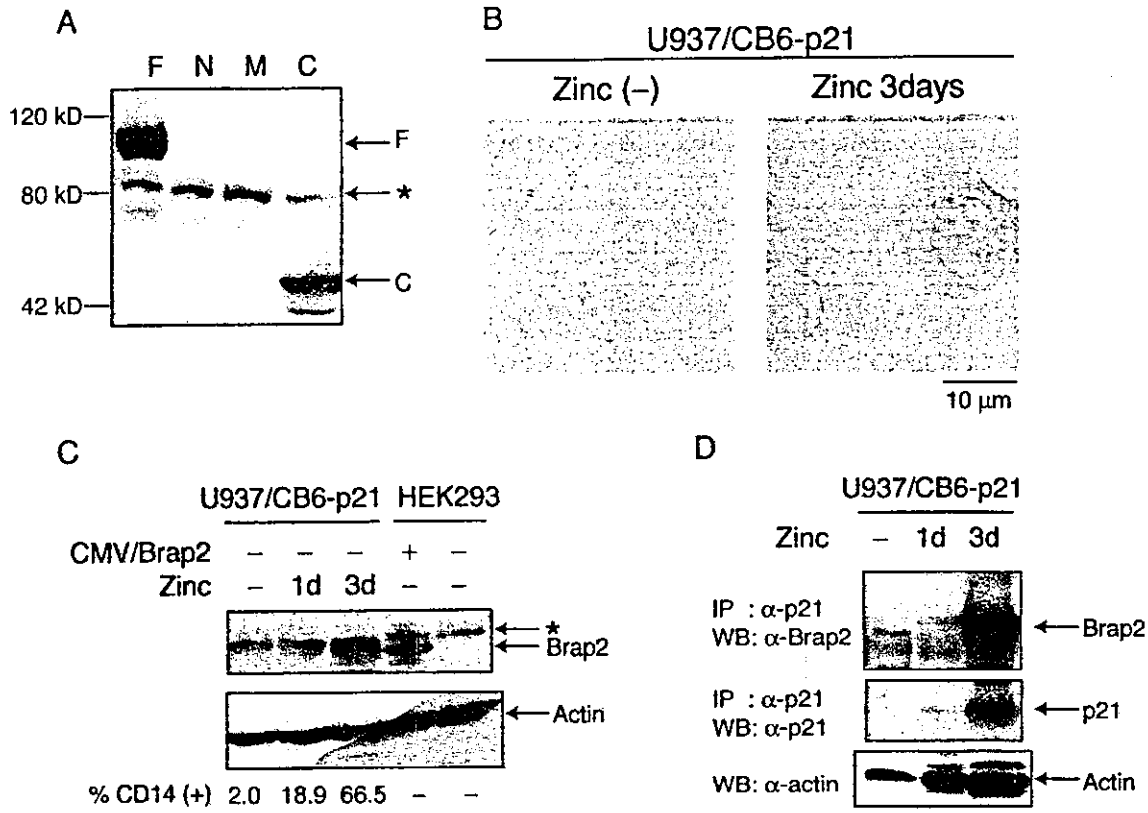

FIG. 7. Expression of Brap2 protein is increased during monocytic differentiation of U937 cells. (A) Anti-Brap2 antibody was generated against the C-terminal portion (aa 423 to 570) of Brap2. This antibody recognizes F or C fragments of the Brap2 fusion protein. Aliquots of the lysates used in the procedures described in the legend to Fig. 5 were subjected to Western blotting with anti-Brap2 antibody. The asterisk indicates a nonspecific band. (B) Immunohistological expression of Brap2 in zinc-treated U937/CB6-p21 cells. (C) Brap2 expression is increased during monocyte differentiation. Cell lysates from U937/CB6-p21 cells treated with 120 μM $ZnSO_4$ for 1 day or 3 days were extracted. As a positive control, HEK293 cells were transfected with pCMV/Brap2. Cell lysates were subjected to Western blotting with anti-Brap2 antibody. The percentage of cells that were CD14 positive is shown at the bottom. (D) Brap2 was coimmunoprecipitated with p21 in differentiating U937/CB6-p21 cells. Zinc-treated U937/CB6-p21 cells were lysed and immunoprecipitated (IP) with anti-p21 antibody. Immune complexes were electrophoresed and subjected to Western blotting (WB) with anti-Brap2 or anti-p21 antibody (top and middle panels). The loading control was subjected to Western blotting with antiactin antibody (bottom panel).

cellular localization of NLS- and/or NES-bearing proteins is controlled by the accessibility of their NLS and/or NES to the transport machinery.

During monocyte differentiation, the cell cycle inhibitory protein p21 translocates from the nucleus to the cytoplasm (3). Interestingly, whereas in the nucleus p21 functions as a cell cycle brake by binding to multicyclin/Cdk complexes and PCNA-DNA polymerase δ subunit (21), in the cytoplasm p21 can promote the assembly of cyclin D/Cdk4 complexes and their nuclear translocation (12). This function is reportedly essential for cyclin D/Cdk4 activation (7). It was previously reported that in monocytes, p21 is expressed in the cytoplasm, where it acts as an inhibitor of apoptosis (3). Another novel function of cytoplasmic p21 associated with increased neurite outgrowth in developing neurons has been recently reported (23). Thus, cytoplasmic p21 exerts biological effects distinct from those of nuclear p21, and it is important to determine the regulatory mechanisms responsible for its cytoplasmic or nuclear expression.

Because p21 is essentially a nuclear protein, it is translated in the cytoplasm and then translocates into the nucleus by means of the NLS. This is not the case in differentiated monocytes where p21 is expressed in cytoplasm. There are at least two possible mechanisms for cytoplasmic expression of p21, one being cytoplasmic retention of p21, i.e., inhibition of its nuclear translocation, and the other being nuclear export of p21. We failed to show involvement of p21 nuclear export in monocytic differentiation because of the lack of appropriate experimental designs. Therefore, the involvement of monocyte-specific nuclear export of p21 cannot be ruled out completely. In the present study, however, we demonstrated that the inhibition of p21 nuclear transport by Brap2 is a possible mechanism for cytoplasmic p21 expression.

Brap2 was shown to be a unique cytoplasmic protein with the ability to bind to both simple and bipartite NLS. Furthermore, Brap2 reportedly possesses a higher NLS binding affinity than importin α (13). This characteristic supports the hypothesis that Brap2 can function as a cytoplasmic retention protein for NLS-bearing molecules by interfering with their interaction with importin α. To our knowledge, p21 is the first partner of Brap2 demonstrated to physically interact with it, leading to the retention of p21 in cytoplasm. It should also be noted that Brap2 expression is upregulated in a differentiation-associated manner in U937 and HL60 cells, thus indicating a coordinated

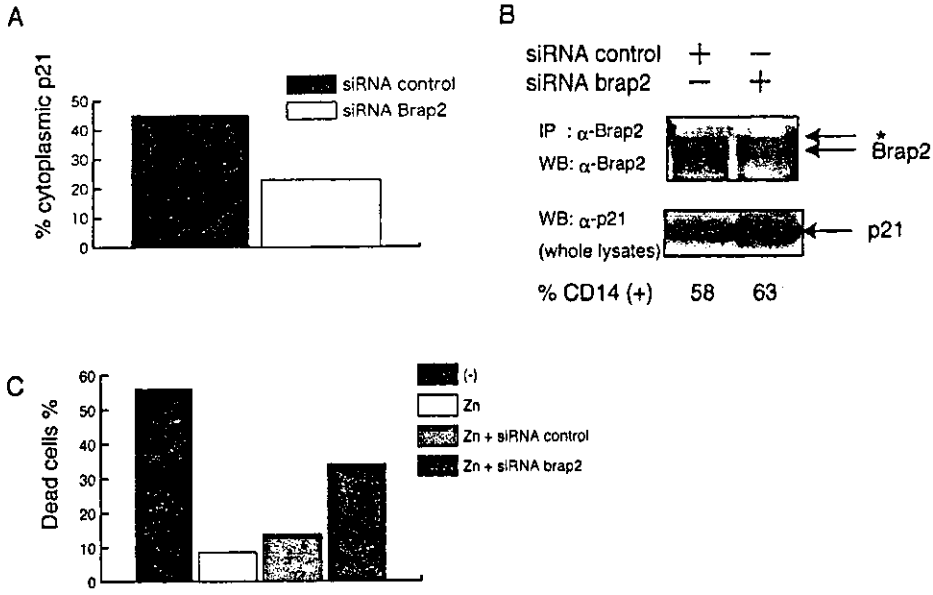

FIG. 8. Inhibition of Brap2 by siRNA does not inhibit p21 expression but reduces cytoprotective activity of cytoplasmic p21. (A) Percentage of cytoplasmic p21-expressing cells in U937/CB6-p21 cells treated with zinc for 3 days in the presence of siRNA. U937/CB6-p21 cells were transfected with control or Brap2-targeting siRNA and then treated with 120 μM $ZnSO_4$ for 3 days. The results from one of three experiments are shown. (B) Brap2 expression was reduced in the presence of siRNA. Cell lysates from U937/CB6-p21 cells treated with zinc for 3 days in the presence of siRNA were extracted. Cell lysates were immunoprecipitated (IP) with anti-Brap2 antibody and subjected to Western blotting (WB) with anti-Brap2. Whole-cell lysates were blotted with anti-p21 antibody, demonstrating significant expression induction of p21 in both transfectants. The percentage of cells that were CD14 positive is shown under the blot. The asterisk indicates a nonspecific band. (C) Inhibition of Brap2 expression by siRNA reduces resistance against hydrogen peroxide-induced apoptosis of differentiated U937/CB6-p21 cells. U937/CB6-p21 cells were transfected with either control or Brap2-targeting siRNA and were cultured with Zn for 3 days. Cells were treated with 300 μM hydrogen peroxide for 16 h. Dead cells were scored by fluorescence-activated cell sorting analysis. The results from one of three experiments are shown.

Brap2 expression is upregulated in a differentiation-associated manner in U937 and HL60 cells, thus indicating a coordinated expression of p21 and Brap2 during monocyte differentiation. Furthermore, treatment with Brap2-targeting siRNA reduced cytoplasmic p21 expression concomitantly with reduction of apoptosis resistance.

In coexpression studies of GFP-p21-NLS in HeLa cells, the transfection efficiency with Brap2 appeared significantly lower than that of mock vector. This lower efficiency is probably because the overexpression of Brap2 is toxic to cells; this toxicity might arise from the fact that Brap2 could target nuclear proteins, whose physiological function is impaired when they are retained in the cytoplasm, thus inhibiting cell survival and/or cell growth. Alternatively, as has been reported recently, Brap2 (IMP) inactivates KSR, a scaffold or adaptor protein that couples activated Raf to its substrate MEK (16), and thus the overexpression of Brap2 may inhibit cell proliferation through inactivating Ras activation signals.

Recently, a mechanism in breast cancer cells for cytoplasmic p21 expression involving the Akt system has been reported (25). Akt phosphorylates at Thr-145 in the NLS of p21 and inhibits nuclear translocation. Breast cancer cells overexpressing HER-2/neu, which activates Akt, could escape from p21-induced cell cycle arrest and acquire apoptosis resistance. It is hypothesized that this represents one of the mechanisms for clonal growth of cancer cells, though it is still controversial in the light of the findings of others (14, 18). Monocyte differentiation is associated with cell cycle arrest, which, in contrast to cell growth systems, is usually examined. In the system using VD_3, we did not detect any phosphorylated active form of Akt (data not shown), though some monocyte differentiation signals such as those induced by TPA could activate Akt (data not shown). These findings make it unlikely that Akt signaling is involved in our system.

Binding to apoptosis signal-regulating kinase 1 (ASK1) exerts at least the cytoprotective ability of p21. ASK1 binds p21 at aa 1 to 140 (3), and Brap2 binds at aa 140 to 164. Thus, ASK1 and Brap2 bind p21 at close but distinct domains. As ASK1 is a cytoplasmic protein, one might speculate that it acts as a cytoplasmic retention protein for p21. However, this seems unlikely for the following reasons: first, the level of ASK1 expression does not change during monocyte differentiation (data not shown), and second, at an early stage of monocyte differentiation (3), p21 expression was detected in the nucleus even in the presence of ASK1. Thus, we hypothesize that during monocyte differentiation, which depends on p21 expression (2), p21 and Brap2 expression are concomitantly induced and the expressed Brap2 protects the NLS of p21, allowing p21 to remain in the cytoplasm and subsequently bind to ASK1.

There may be many other Brap2-like proteins, localizing to cytoplasm and interacting with NLS motifs. Thus, cytoplasmic retention proteins may comprise a unique functional family. They function as inhibitors and/or sequestering factors for nuclear proteins but mediate novel biological functions of the nuclear proteins in the cytoplasm.

ACKNOWLEDGMENTS

This work was supported by a Grant-in-Aid for Cancer Research from the Ministry of Health and Welfare, Japan, as part of a comprehensive 10-year strategy for cancer control; by a Grant-in-Aid from the Ministry of Education, Science and Culture, Japan; by a grant from the Japan Leukemia Research Fund; and by the Italian Association for Cancer Research (AIRC) and Telethon grants E.337 and E764.

REFERENCES

1. **Alt, J. R., J. L. Cleveland, M. Hannink, and J. A. Diehl.** 2000. Phosphorylation-dependent regulation of cyclin D1 nuclear export and cyclin D1-dependent cellular transformation. Genes Dev. **14**:3102–3114.
2. **Asada, M., T. Yamada, K. Fukumuro, and S. Mizutani.** 1998. p21Cip1/WAF1 is important for differentiation and survival of U937 cells. Leukemia **12**:1944–1950.
3. **Asada, M., T. Yamada, H. Ichijo, D. Delia, K. Miyazono, K. Fukumuro, and S. Mizutani.** 1999. Apoptosis inhibitory activity of cytoplasmic p21(Cip1/WAF1) in monocytic differentiation. EMBO J. **18**:1223–1234.
4. **Bettens, F., E. Schlick, W. Farrar, and F. Ruscetti.** 1986. 1,25-Dihydroxycholecalciferol-induced differentiation of myelomonocytic leukemic cells unresponsive to colony stimulating factors and phorbol esters. J. Cell. Physiol. **129**:295–302.
5. **Bromleigh, V. C., and L. P. Freedman.** 2000. p21 is a transcriptional target of HOXA10 in differentiating myelomonocytic cells. Genes Dev. **14**:2581–2586.
6. **Chen, Y., C.-F. Chen, D. J. Riley, D. C. Allred, P.-L. Chen, D. Von Hoff, C. K. Osborne, and W.-H. Lee.** 1995. Aberrant subcellular localization of BRCA1 in breast cancer. Science **270**:789–791.
7. **Cheng, M., P. Oliver, J. A. Diehl, M. Fero, M. F. Roussel, J. M. Roberts, and C. J. Sherr.** 1999. The p21 Cip1 and p27 Kip1 CDK 'inhibitors' are essential activators of cyclin D-dependent kinases in murine fibroblasts. EMBO J. **18**:1571–1583.
8. **Cyert, M. S.** 2001. Regulation of nuclear localization during signaling. J. Biol. Chem. **276**:20805–20808.
9. **Elbashir, S. M., J. Harborth, W. Lendeckel, A. Yalcin, K. Weber, and T. Tuschl.** 2001. Duplexes of 21-nucleotide RNAs mediate RNA interference in cultured mammalian cells. Nature **411**:494–498.
10. **Jiang, H., J. Lin, Z.-Z. Su, F. R. Collart, E. Huberman, and P. B. Fisher.** 1994. Induction of differentiation in human promyelocytic HL-60 leukemia cells activates p21, WAF1/CIP1, expression in the absence of p53. Oncogene **9**:3397–3406.
11. **Kuersten, S., M. Ohno, and I. W. Mattaj.** 2001. Nucleocytoplasmic transport: Ran, beta and beyond. Trends Cell Biol. **11**:497–503.
12. **LaBaer, J., M. D. Garrett, L. F. Stevenson, J. M. Slingerland, C. Sandhu, H. S. Chou, A. Fattaey, and E. Harlow.** 1997. New functional activities for the p21 family of CDK inhibitors. Genes Dev. **11**:847–862.
13. **Li, S., C. Y. Ku, A. A. Farmer, Y. S. Cong, C. F. Chen, and W. H. Lee.** 1998. Identification of a novel cytoplasmic protein that specifically binds to nuclear localization signal motifs. J. Biol. Chem. **273**:6183–6189.
14. **Li, Y., D. Dowbenko, and L. A. Lasky.** 2002. AKT/PKB phosphorylation of p21Cip/WAF1 enhances protein stability of p21Cip/WAF1 and promotes cell survival. J. Biol. Chem. **277**:11352–11361.
15. **Liu, M., M. H. Lee, M. Bommakanti, and L. P. Freedman.** 1996. Transcriptional activation of the Cdk inhibitor p21 by vitamin D3 leads to the differentiation of the myelomonocytic cell line U937. Genes Dev. **10**:142–153.
16. **Matheny, S. A., C. Chen, R. L. Kortum, G. L. Razidlo, R. E. Lewis, and M. A. White.** 2004. Ras regulates assembly of mitogenic signalling complexes through the effector protein IMP. Nature **427**:256–260.
17. **Poon, R. Y. C., and T. Hunter.** 1998. Expression of a novel form of p21Cip1/Waf1 in UV-irradiated and transformed cells. Oncogene **16**:1333–1343.
18. **Rössig, L., A. S. Jadidi, C. Urbich, C. Badorff, A. M. Zeiher, and S. Dimmeler.** 2001. Akt-dependent phosphorylation of $p21^{Cip1}$ regulates PCNA binding and proliferation of endothelial cells. Mol. Cell. Biol. **21**:5644–5657.
19. **Rots, N. Y., M. Liu, E. C. Anderson, and L. P. Freedman.** 1998. A differential screen for ligand-regulated genes: identification of *HoxA10* as a target of vitamin D_3 induction in myeloid leukemic cells. Mol. Cell. Biol. **18**:1911–1918.
20. **Scully, R., and D. M. Livingston.** 2000. In search of the tumour-suppressor functions of BRCA1 and BRCA2. Nature **408**:429–432.
21. **Sherr, C. J., and J. M. Roberts.** 1995. Inhibitors of mammalian G1 cyclin-dependent kinases. Genes Dev. **9**:1149–1163.
22. **Steinman, R. A., B. Hoffman, A. Iro, C. Guillouf, D. A. Liebermann, and M. E. El-Houseini.** 1994. Induction of p21(WAF1/CIP1) during differentiation. Oncogene **9**:3389–3396.
23. **Tanaka, H., T. Yamashita, M. Asada, S. Mizutani, H. Yoshikawa, and M. Tohyama.** 2002. Cytoplasmic p21Cip1/WAF1 regulates neurite remodeling by inhibiting Rho-kinase activity. J. Cell Biol. **158**:321–329.
24. **Toyoshima-Morimoto, F., E. Taniguchi, N. Shinya, A. Iwamatsu, and E. Nishida.** 2001. Polo-like kinase 1 phosphorylates cyclin B1 and targets it to the nucleus during prophase. Nature **410**:215–220.
25. **Zhou, B. P., Y. Liao, W. Xia, B. Spohn, M. H. Lee, and M. C. Hung.** 2001. Cytoplasmic localization of p21Cip1/WAF1 by Akt-induced phosphorylation in HER-2/neu-overexpressing cells. Nat. Cell Biol. **3**:245–252.

Available online at www.sciencedirect.com
SCIENCE DIRECT
Enzyme and Microbial Technology 35 (2004) 519–524
ENZYME and MICROBIAL TECHNOLOGY
www.elsevier.com/locate/enzmictec

Expression and amplification of glutamine synthetase gene endows HepG2 cells with ammonia-metabolizing activity for bioartificial liver support system

Takeshi Omasa[a,*], Mitsugu Yamanaka[a], Naoko Tanimura[a], Yoshio Katakura[a], Michimasa Kishimoto[a], Ken-ichi Suga[a], Shin Enosawa[b]

[a] *Department of Biotechnology, Osaka University, 2-1 Yamada-oka Suita, Osaka 565-0871, Japan*
[b] *National Research Institute for Child Health and Development, Setagaya, Tokyo 154-8509, Japan*

Abstract

To establish the ammonia-metabolizing cell lines for a bioartificial liver support system, CHO-K1 and HepG2 were transformed with pBK-CMV-GS vector that contains glutamine synthetase (*gs*) gene. The recombinant cell lines were selected under the various concentrations of glutamine synthetase inhibitor, methionine sulfoximine (MSX). The host CHO-K1 and HepG2 cell lines produces ammonia, but the both MSX tolerable CHO (GS-CHO) and HepG2 (GS-HepG2) cell lines endowed with the high GS activity could metabolize the ammonium from medium. The ammonia-metabolizing activity of CHO and HepG2 cell was about one-fourth of that of primary hepatocyte.

Keywords: Ammonia-metabolizing activity; HepG2 cell; CHO; Bioartificial liver support system; Gene amplification

1. Introduction

A hybrid bioartificial liver support (BAL) system, composed of artificial materials and living cells, was developed for stopgap use in patients with hepatic failure [1–5]. In these systems, primary xenogeneic hepatocytes have heretofore been the predominant cell type used to support human liver functions in BAL systems. These BAL systems are extremely effective for short-term use (a few days), but are unsuitable for long-term use (more than 1 week), because of the short life span of the primary hepatocyte. In designing a BAL system for a long-term use, the most important factor is the use of a highly functional and long-term stable human liver cell line [6]. Moreover, because of the risk of zoonoses, the use of primary hepatocyte is still ongoing debate [7]. From the viewpoint of BAL evaluation, the safety requirement is most important factor requiring in BAL system [8]. Hepatoma-derived cell lines are suitable for long-term use because of their infinite capacity for proliferation and it is easy to control and verify the cell line quality. Recently, human hepatoma-derived cell line was used as BAL system and effective for acute liver failure [9,10]. However, the hepatoma-derived cell line frequently loses some of the liver cell functions, especially its "ammonia-metabolizing" activity [11,12]. Ammonia is considered to be one of the major causes of hepatic encephalopathy, which is among the most serious pathophysiological features of fulminant hepatic failure [13,14]. Hemodialysis and/or plasmapheresis have been used for ammonia removal but neither can be effective for selective removal of ammonia.

In the liver, selective removal of ammonia is accomplished mainly by the urea cycle. However, it is difficult to apply the urea cycle for the removal of ammonia using recombinant DNA techniques, because the cycle involves five complex enzyme reactions. While, the glutamine synthetase reaction is used as a secondary metabolic pathway for the removal of ammonia in the liver [15,16]. Moreover, glutamine synthetase gene can be amplified in the Chinese hamster ovary (CHO) cells under selection by the glutamine synthetase inhibitor, methionine sulfoximine

* Corresponding author. Tel.: +81 6 6879 7437; fax: +81 6 6879 7439.
E-mail address: omasa@bio.eng.osaka-u.ac.jp (T. Omasa).

0141-0229/$ – see front matter © 2004 Elsevier Inc. All rights reserved.
doi:10.1016/j.enzmictec.2004.08.027

(MSX) [17,18]. Based on these studies, we supposed that an expression and amplification of glutamine synthetase gene could endow cell with ammonia-metabolizing activity. In this study, we attempted to give ammonia-metabolizing activity to CHO and hepatoma-derived HepG2 cell lines by recombination and gene amplification of the glutamine synthetase gene. While, in case of gene amplification in HepG2, only CAD gene amplification was reported [19]. This study is first trial of *gs* gene amplification in HepG2 cell line.

2. Materials and methods

2.1. Cell line, medium, and construction of recombinant cell lines

The cell lines employed in the experiments were the CHO-K1 (RCB0285) and HepG2 (RCB0459) cell lines. The expression vector, pBK-CMV-GS, was constructed by insertion of the Chinese hamster glutamine synthetase gene into the pBK-CMV (Stratagene 212209) vector (Fig. 1). The CHO-K1 and HepG2 cells were transformed with the pBK-CMV-GS vector using the lipofection method (DOSPER liposomal transfection reagent kit, Boehringer-Mannheim). The tissue culture medium was RDF (HO) medium [20] containing glucose (2.58 g l^{-1}), glutamine (333 mg l^{-1}) and 10% dialyzed fetal bovine serum. The selection medium contains glutamic acid (336 mg l^{-1}) and NH_4Cl (122 mg l^{-1}) instead of glutamine, and Geneticin (G418; 500 μg l^{-1}) for neomycin selection. The recombinant cells were selected under various concentrations of the glutamine synthetase inhibitor, methionine sulfoximine. Over a 4-month selection period, the MSX concentrations in the medium was gradually increased from 25 to 5000 μM for the CHO cell line and from 10 to 1000 μM for the HepG2 cell line, respectively. The each cell line was cloned by colony ring method. In case of the experimental evaluation of the ammonia-metabolizing activity in each established cell line, the ammonia concentration was adjusted in the range of 0–1 mM in each experiment. The constructed *gs* recombinant HepG2 cell line (GS-HepG2) was registered in cell bank (Riken Bioresource Center, Tsukuba, Japan) as a RCB 1680.

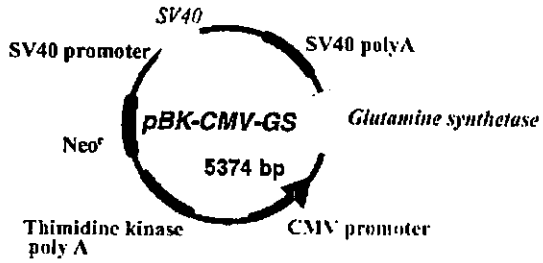

Fig. 1. The structure of pBK-CMV-GS vector.

2.2. Cultivation and evaluation of ammonia-metabolizing, glutamine synthetase and 7-ethoxycoumarin activities

Evaluation of the ammonia-metabolizing activity was performed in T-flask culture (medium volume 90 ml). The cell concentration was measured by photomicrography. The glucose, lactate, glutamine, and ammonia concentrations were analyzed using enzyme reaction as described previously [20,21]. Amino acids concentrations were measured by PICO-TAG HPLC system (Waters) using PITC-amino acids. Urea concentration was measured using enzyme reaction kit (Wako UN278-0481). The kinetic parameters were calculated within 95% confidence limits by the integration procedure taking into consideration sampling loss and natural degradation of glutamine [20,21]. The coefficient of variance in every measurement was less than 5%, especially, in the case of ammonia, it was less than 1%. Glutamine synthetase activity in crude extracts of the cells was determined by the γ-glutamyl transfer reaction [22]. Relative copy number of glutamine synthetase gene in established cell was determined by dot blotting using DIG-DNA labeling and detection kit (Bio-Rad) described previously [23]. Determination of copy number was performed using densitometer (Shimadzu CS-9300PC). The drug-metabolizing activity of HepG2 cells was determined based on the 7-ethoxycoumarin-metabolizing activity [24].

3. Results and discussion

3.1. Expression and gene amplification of glutamine synthetase in CHO

CHO-K1 and hepatoma-derived HepG2 cells were transformed with the pBK-CMV-GS vector containing the glutamine synthetase (*gs*) gene with the CMV promoter. *gs* gene amplification efficiency was strongly influenced by the increase in MSX concentration. In this study, based on the *dhfr*-MTX gene amplification techniques reported in our previous work [23], the MSX concentration was gradually increased during selection (Fig. 2). In case of 500 and 1000 μM in step 2 and 5000 μM in step 3, it take long time for reaching about 80% confluent condition. Initially, the host CHO-K1 cell ex-

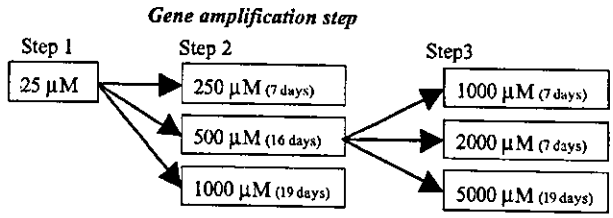

Fig. 2. Increasing pattern of MSX concentration in MSX-tolerant recombinant CHO cells (days: 80% confluent time from stepwise increase of MSX concentration).

hibited very weak GS activity (2.0×10^{-7} units cell^{-1}); at the end of the selection period, the GS activity increased 30-fold compared with that in the host CHO-K1 cell line (about 60×10^{-7} units cell^{-1}). However, under more than 1000 μM MSX concentration, GS activity could not be increased further. Among the 500 or 1000 μM MSX-tolerant cell lines, we established the 500 μM MSX-tolerant cell line (GS-CHO 500 μM) which exhibited the highest GS activity (130×10^{-7} units cell^{-1}) was selected by the colony ring method.

3.2. Expression and gene amplification of glutamine synthetase in HepG2

Similar *gs* amplification was carried out in the HepG2 cell line. Since no studies have so far reported *gs* gene amplification in the HepG2 cell line, the similar method as that used for the CHO cell line, using increasing concentrations of MSX was applied to the HepG2 cell line (Fig. 3). In case of 500 and 1000 μM MSX concentration in step 3, once we obtained cell lines but they were unstable. Finally, we lost these constructed cell line in step 3. At the underlined conditions of MSX selection in Fig. 3, we could not establish any survival cell lines. Comparing with *gs* gene amplification in CHO, it was difficult to obtain high MSX tolerable cell line. Moreover, it takes a longer time for constructing the cell line. In order to verify the gene amplification of *gs* gene, the GS activity and the relative copy number of the established cell lines were investigated (Fig. 4). With increase of MSX concentration in the medium, the GS activity increased, to five-fold in the 500 μM MSX that in the 10 μM MSX tolerable HepG2 cell line. The copy number of *gs* gene also increased to two-fold. Among the MSX-tolerant cell lines, we selected the 200 and 300 μM MSX-tolerant cell line based not only on the GS activity but also on the growth rate, because the growth rate of 500 μM MSX-tolerant cell lines is too low for ammonia-metabolizing experiment.

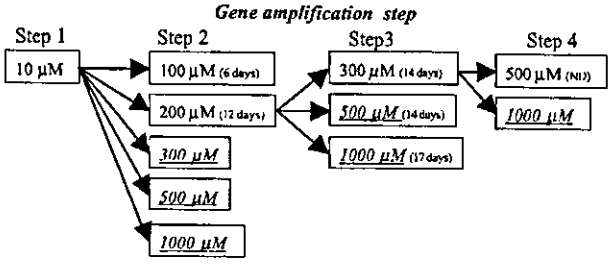

Fig. 3. Increasing pattern of MSX concentration in MSX-tolerant recombinant HepG2 cells (days: 80% confluent time from stepwise increase of MSX concentration; underline: we could not establish cell line; ND: not determined confluent time).

3.3. Ammonia-metabolizing activities of recombinant CHO and HepG2

The ammonia-metabolizing activities of constructed GS-CHO and GS-HepG2 cell lines were evaluated. The time course of changes in cell concentration, ammonia concentration, glucose, glutamine and glutamate with addition of 1 mM ammonia concentration are shown in Fig. 5. Wild CHO-K1 and HepG2 cell lines produced ammonia during cultivation, while the constructed recombinant cell lines consumed ammonia and produced glutamine during cultivation, due to GS activity. The consumption of glutamate in GS-HepG2 was quite compatible to that of wild HepG2. The specific growth rate of constructed 200 μM GS-HepG2 is $0.0201 \pm 0.0105\ h^{-1}$. This value corresponded the 34 h doubling time and was lower than that of 500 μM MSX-tolerant GS-CHO cell line (about 20 h doubling time). The time course of amino acids concentrations were shown in Fig. 6. The amino acid profile during cultivation was classified into the type which were to decrease the concentration (Arg, Ile, Leu, Val, Pro, Ser, Met, Cys) and other one which was slightly to increase or to keep constant concentration (Lys, Tyr, Gly, His, Asp, Thr, Ala). In the hepatic failure, the amino acid balance parameter, the molar ratio of branched amino acid to aromatic amino acid ((Val + Leu + Ile)/(Tyr + Phe); Fischer's ratio) is important parameter [25,26]. Normalization of the Fischer's ratio correlates with clinical improvement. By increase of this parameter, the uptake of aromatic amino acids into a brain is promoted and causes hepatic encephalopathy [27]. In these experiments, this parameter slightly decreased during cultivation. During the cultivation, the urea could not be detected in the medium of recombinant HepG2. In order to compare the ammonia-metabolizing activity quantitatively, the specific ammonia consumption rates (ammonia-metabolizing activity per unit cell per hour) of the constructed cell lines were calculated, respectively, as shown in Table 1, wild-type CHO-

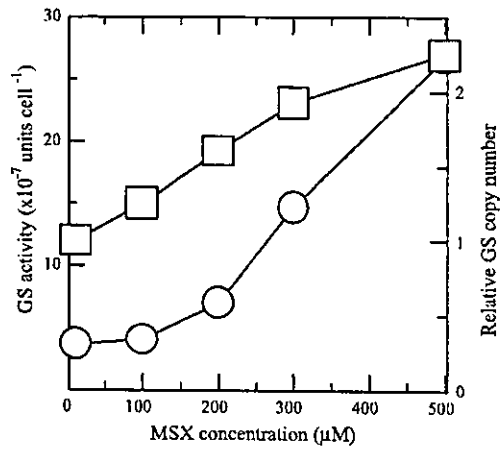

Fig. 4. The relationship between GS activity (○), the relative copy number of the established cell lines (□) and MSX concentration. The copy number was normalized based on that in 10 μM MSX concentration.

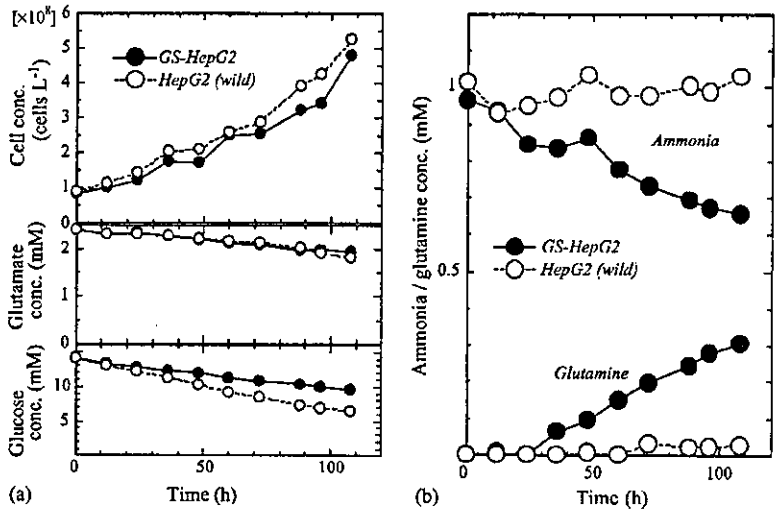

Fig. 5. Time courses in HepG2 (wild) and GS-HepG2 (200 μM MSX-tolerant) cell lines with addition of 1 mM ammonia concentration.

K1 and HepG2 cell lines and primary hepatocytes (Table 1). The specific ammonia consumption rates in the constructed CHO and HepG2 cell lines were about one-fourth of the rate in primary hepatocytes. The ammonia-metabolizing activity was also evaluated under 0.1 mM ammonia concentration (this concentration is approximately the same as that seen in hepatic failure patients). The constructed cell line reduced ammonia concentration to 0.05 mM, corresponding normal ammonia concentration in human blood, immediately and the ammonia-metabolizing activity in 0.1 mM was one-third of that under 1 mM ammonia concentration (Table 1). Although recombinant CHO cells exhibited higher GS activity than recombinant HepG2 cells, HepG2 cells exhibited almost equivalent ammonia-metabolizing activity to that of recombinant CHO cells. In other words, the *gs* gene was not strongly amplified in HepG2 cells. According to the gene amplification mechanism, cell growth is necessary for amplification. In the case of HepG2 cells, the growth rate of MSX-tolerant cell lines was decreased. Therefore, the gene amplification efficiency might be lower than that in the recombinant CHO cell line.

In order to improve the ammonia-metabolizing activity, we investigated the effects of increase of glutamate and zinc concentration. It was reported that oral zinc supplementation improve hepatic encephalopathy for cirrhotic patients [28]. The oral zinc supplementation activated the glutamine synthetase and prevented hepatic encephalopathy [29]. To enhance ammonia-metabolizing activity, we increased the zinc ($ZnSO_4 \cdot 7H_2O$) concentration in the medium. Among, 0.215 mg l^{-1} (control), 5, 10, 50, 120, and 300 mg l^{-1} zinc

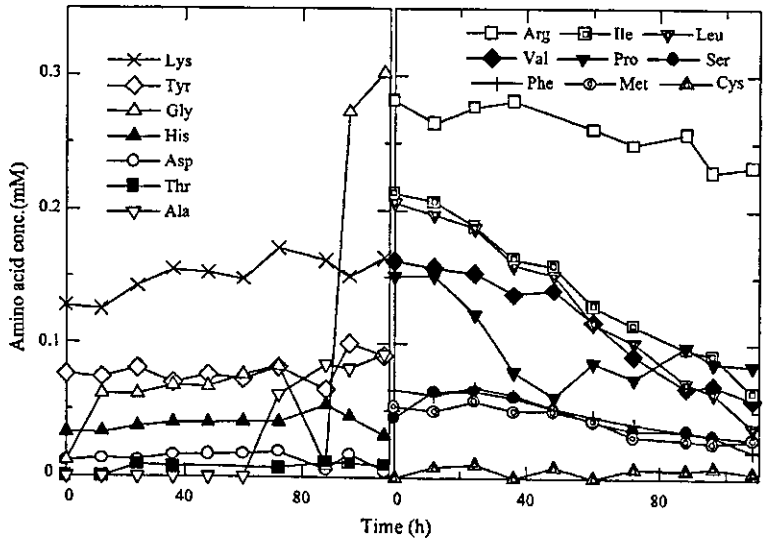

Fig. 6. Time courses of changes in amino acids in GS-HepG2 (200 μM MSX-tolerant) cell lines with addition of 1 mM ammonia concentration.

Table 1
Comparison of specific ammonia consumption rates between primary hepatocytes and recombinant CHO and HepG2 cell lines

	Initial ammonia concentration (mM)	Specific ammonia consumption rate ($\times 10^{-13}$ mol cell^{-1} h^{-1})
GS-CHO (500 μM MSX-tolerant) cell line	0.89	0.24 ± 0.016
	0.11	0.078 ± 0.059
	0.11[a]	0.12 ± 0.015
	0.13[b]	0.24 ± 0.015
CHO-K1 (wild)	0.91	−0.21 ± 0.037
	0.11	−0.18 ± 0.037
GS-HepG2 (300 μM MSX-tolerant) cell line	0.93	0.23 ± 0.051
	0.87[a]	0.34 ± 0.005
GS-HepG2 (200 μM MSX-tolerant) cell line	0.96	0.14 ± 0.017
	0.12	0.034 ± 0.0037
HepG2 (wild)	1.01	−0.027 ± 0.0091
	0.10	−0.27 ± 0.018
Rat primary hepatocytes[c]	1.0	0.963

[a] Zinc enrichment (10 mg l^{-1}).
[b] Glutamate enrichment (7.41 mM).
[c] Primary hepatocyte in a PUF/Spheroid culture system [35].

enhancement cultivations using 500 μM MSX-tolerant GS-CHO cell line under 0.1 mM ammonia concentration, the GS-CHO cell line could not survive more than 50 mg l^{-1} concentrations. In case of 10 mg l^{-1} zinc supplementation, the ammonia-metabolizing activity was enhanced compared with normal culture condition (Table 1). Glutamate is major substrate for enzyme reaction in glutamine synthetase. In order to enhance the ammonia-metabolizing activity, the 7.41 and 15 mM glutamate enrichment culture were performed under 0.1 mM ammonia concentration. In case of 15 mM glutamate concentration, cell growth was inhibited. The ammonia-metabolizing activity was significantly enhanced by the addition of 7.41 mM glutamate addition (Table 1). In case of GS-HepG2 (200 μM MSX-tolerant) cell line, the 7.41 mM glutamate addition enhanced the 1.5 times higher ammonia-metabolizing activity. This value is one-third of the primary hepatocyte.

The hepatoma-derived HepG2 cell line retains some of the functions of normal liver. In our previous investigation, the ammonia-metabolizing activity was easily lost in hepatoma-derived cell lines, but drug-metabolizing activity was still retained. Compared with other hepatoma-derived cell lines, the HepG2 cell line exhibited higher drug-metabolizing (7-ethoxycoumarin-metabolizing) activity. This activity is representative parameter of P450 drug metabolism. The drug-metabolizing activity in the constructed GS-HepG2 (200 μM MSX-tolerant) cell line was maintained at the same level (4.7 pmol 10^6 cells^{-1} h^{-1}) as that in the host HepG2 cell line despite the recombination and 4-month selection for gene amplification. GS-HepG2 cell line also kept inducibility of P4503A4 enzyme by rifampicin (data not shown). In the case of primary hepatocytes, the drug-metabolizing activity was high but disappeared within 1 week of isolation from the liver [30]. By using our GS-HepG2 (300 μM MSX-tolerant) cell lime, we constructed bioartificial liver support system with circulatory flow bioreactor [31]. Using this bioartificial liver support system, we successfully cultivated GS-HepG2 cell line for more than 60 days [32]. Finally, the bioartificial liver support system could significantly improve the survival time of pigs with ischemic liver failure comparing with normal HepG2 or bioartificial liver support system without cells [33,34].

The *gs* gene amplification system can be used to amplify not only the *gs* gene but also other useful genes, using a tandem vector. It is possible to obtain a HepG2 cell line, with not only ammonia-metabolizing activity but also other liver functions, by gene amplification.

References

[1] Rozga J, Demetriou AA. Evolution and future perspectives. ASAIO J 1995;41:831–7.
[2] Sauer IM, Obermeyer N, Kardassis D, Theruvath T, Gerlach JC. Development of a hybrid liver support system. Ann N Y Acad Sci 2001;944:308–19.
[3] Hu WS, Friend JR, Wu FJ, Sielaff T, Peshwa MV, Lazar A, et al. Development of a bioartificial liver employing xenogeneic hepatocytes. Cytotechnology 1997;23:29–38.
[4] Nyberg SL, Misra SP. Hepatocyte liver-assist systems—a clinical update. Mayo Clin Proc 1998;73:765–71.
[5] Friedman AL. Why bioartificial liver support remains the Holy Grail. ASAIO J 1998;44:241–3.
[6] Stange J, Mitzner S. Cell sources for bioartificial liver support. Int J Artif Organs 1996;19:14–7.
[7] Strain AJ, Neuberger JM. A bioartificial liver—state of the art. Science 2002;295:1005–9.
[8] Omasa T, Kishimoto M, Kawase M, Yagi K. An attempt at decision making in tissue engineering: reactor evaluation using the analytic hierarchy process (AHP). Biochemical Eng J 2004;20:173–9.
[9] Sussman NL, Killy JH. Improved liver function following treatment with an extracorporeal liver assist device. Artif Organs 1993;17:27–30.

[10] Ellis AJ, Hughes RD, Wendon JA, Dunne J, Langley PG, Kelly JH, et al. Pilot-controlled trial of the extracorporeal liver assist device in acute liver failure. Hepatology 1996;24:1446–51.
[11] Enosawa S, Suzuki S, Kakefuda T, Amemiya H. Examination of 7-ethoxycoumarin deethylation and ammonia removal activities in 31 hepatocyte cell lines. Cell Transplant 1996;5:S39–40.
[12] Wang L, Sun J, Li L, Mears D, Horvat M, Sheil AG. Comparison of porcine hepatocytes with human hepatoma (C3A) cells for use in a bioartificial liver support system. Cell Transplant 1998;7:459–68.
[13] Mousseau DD, Butterworth RF. Current theories on the pathogenesis of hepatic encephalopathy. Proc Soc Exp Biol Med 1994;206:329–44.
[14] Wakabayashi H, Kuwabara Y, Murata H, Kobashi K, Watanabe A. Measurement of the expiratory ammonia concentration and its clinical significance. Metab Brain Dis 1997;12:161–9.
[15] Haussinger D. Nitrogen metabolism in liver: structural and functional organization and physiological relevance. Biochem J 1990;267:281–90.
[16] Haussinger D. Hepatocyte heterogeneity in glutamine and ammonia metabolism and the role of an intercellular glutamine cycle during ureogenesis in perfused rat liver. Eur J Biochem 1983;133:269–75.
[17] Cockett MI, Bebbington CR, Yarranton GT. High level expression of tissue inhibitor of metalloproteinases in Chinese hamster ovary cells using glutamine synthetase gene amplification. Biotechnology 1990;8:662–7.
[18] Omasa T. Gene amplification and its application in cell and tissue engineering. J Biosci Bioeng 2002;94:600–5.
[19] Conner EA, Wirth PJ. Protein alterations associated with gene amplification in cultured human and rodent cells. Electrophoresis 1996;17:1257–64.
[20] Omasa T, Ishimoto M, Higashiyama K, Shioya S, Suga K. The effects of glutamine concentration on growth and monoclonal antibody production in fed-batch operation. Cytotechnology 1992;8:75–84.
[21] Omasa T, Higashiyama K, Shioya S, Suga K. Effect of lactate concentration on hybridoma culture in lactate-controlled fed-batch operation. Biotechnol Bioeng 1992;39:556–64.
[22] Rowe WB, Ronzio RA, Wellener VP, Meister A. Glutamine synthetase (sheep brain). Methods Enzymol 1970;17a:901–10.
[23] Yoshikawa T, Nakanishi F, Ogura Y, Oi D, Omasa T, Katakura Y, et al. Amplified gene location in chromosomal DNA affected recombinant protein production and stability of amplified genes. Biotechnol Prog 2000;16:710–5.
[24] Miller NE, Halpert J. Analogues of chloramphenicol as mechanism-based inactivators of rat liver cytochrome P-450: modifications of the propanediol side chain, the *p*-nitro group, and the dichloromethyl moiety. Mol Pharmacol 1986;29:391–8.
[25] Soeters PB, Fischer JE. Insulin, glucagon, amino acid imbalance, and hepatic encephalopathy. Lancet 1976;308:880–2.
[26] Chen Z, Ding Y, Xu Q, Yu D. Bioartificial liver inoculated with porcine hepatocyte spheroids for treatment of canine acute liver failure model. Artif Organs 2003;27:613–22.
[27] Denis J, Delorme ML, Boschat M, Nordlinger B, Opolon P. Respective roles of ammonia, amino acids, and medium-sized molecules in the pathogenesis of experimentally induced acute hepatic encephalopathy. J Neurochem 1983;40:10–9.
[28] Reding P, Duchateau J, Bataille C. Oral zinc supplementation improves hepatic encephalopathy. Results of a randomised controlled trial. Lancet 1984;324:493–5.
[29] Yoshida Y, Higashi T, Nouso K, Nakatsukasa H, Nakamura SI, Watanabe A, et al. Effects of zinc deficiency/zinc supplementation on ammonia metabolism in patients with decompensated liver cirrhosis. Acta Med Okayama 2001;55:349–55.
[30] Edwards AM, Glistak ML, Lucas CM, Wilson PA. 7-Ethoxycoumarin deethylase activity as a convenient measure of liver drug metabolizing enzymes: regulation in cultured rat hepatocytes. Biochem Pharmacol 1984;33:1537–46.
[31] Enosawa S, Miyashita T, Suzuki S, Li XK, Tsunoda M, Amemiya H, et al. Long-term culture of glutamine synthetase-transfected HepG2 cells in circulatory flow bioreactor for development of a bioartificial liver. Cell Transplant 2000;9:711–5.
[32] Miyashita T, Enosawa S, Suzuki S, Tamura A, Tanaka H, Amemiya H, et al. Development of a bioartificial liver with glutamine synthetase-transduced recombinant human hepatoblastoma cell line HepG2. Transplant Proc 2000;32:2355–8.
[33] Enosawa S, Miyashita T, Fujita Y, Suzuki S, Amemiya H, Omasa T, et al. In vivo estimation of bioartificial liver with recombinant HepG2 cells using pigs with ischemic liver failure. Cell Transplant 2001;10:429–33.
[34] Enosawa S, Miyashita T, Tanaka H, Li X, Suzuki S, Amemiya H, et al. Prolongation of survival of pigs with ischemic liver failure by treatment with a bioartificial liver using glutamine synthetase transfected recombinant HepG2. Transplant Proc 2001;33:1945–7.
[35] Ijima H, Matsushita T, Funatsu K. Development of a hybrid type artificial liver using PUF/Sheroid culture system of adult hepatocytes. Jpn J Artif Organs 1993;22:171–6.

Sensors and Materials, Vol. 16, No. 5 (2004) 241– 254
MYU Tokyo

S & M 0562

Detection of Protein Conformation under Stress Conditions Using Liposomes As Sensor Materials

Ryoichi Kuboi, Toshinori Shimanouchi, Makoto Yoshimoto[1] and Hiroshi Umakoshi

Department of Chemical Science and Engineering, Graduate School of Engineering Science, Osaka University, 1-3 Machikaneyama-cho, Toyonaka, Osaka 560-8531, Japan
[1]Department of Applied Chemistry and Chemical Engineering, Faculty of Engineering, Yamaguchi University, 2-16-1 Tokiwadai, Ube 755-8611, Japan

Sensors and Materials

MYU

Sensors and Materials, Vol. 16, No. 5 (2004) 241– 254
MYU Tokyo

S & M 0562

Detection of Protein Conformation under Stress Conditions Using Liposomes As Sensor Materials

Ryoichi Kuboi*, Toshinori Shimanouchi, Makoto Yoshimoto[1] and Hiroshi Umakoshi

Department of Chemical Science and Engineering, Graduate School of Engineering Science, Osaka University, 1-3 Machikaneyama-cho, Toyonaka, Osaka 560-8531, Japan
[1]Department of Applied Chemistry and Chemical Engineering, Faculty of Engineering, Yamaguchi University, 2-16-1 Tokiwadai, Ube 755-8611, Japan

(Received April 7, 2004; accepted September 27, 2004)

Key words: molten-globule (MG) state, liposome-protein interaction, calcein release, membrane perturbation, membrane fluidity, local hydrophobicity, immobilized liposome chromatography

Calcein release from liposomes was analyzed kinetically in the presence of various proteins under the stress condition. In the case of bovine carbonic anhydrase (CAB), a significant release of calcein was observed at pH 4. The conformational change of CAB from the native to the molten-globule (MG) state was confirmed using an aqueous two-phase partitioning method and immobilized liposome chromatography. The CAB-liposome interaction was maximum at a specific pH (4.0), where the CAB conformation was an MG-like state. The results may show that the hydrophobic interaction between CAB and liposomes enhances the perturbation of the liposome membrane, leading to a significant release of calcein from liposomes. These phenomena depended not only on the characteristics of proteins (local hydrophobicity, LH_{pr}) but also on the dynamic properties of liposomes (membrane fluidity). These results obtained with CAB may be extended to other proteins. The manner of protein-induced calcein release was classified into at least two types. Calcein release due to the addition of proteins having either disulfide bonds or being rich in beta-sheet structure was not observed. On the contrary, a significant release of calcein was observed in the case of a reduced protein with a cleaved disulfide bond and in the case of a protein with relatively a low content of beta-sheet structure. These findings suggest that a liposome containing calcein can be used as an effective sensor element for the detection of proteins having large structural fluctuations.

*Corresponding author, e-mail address: kuboi@cheng.es.osaka-u.ac.jp

1. Introduction

Studies of the function of cell membranes have attracted many researchers because environmental signals (stimuli or stress) are normally recognized on the membrane surface and responses of the cell are induced there. A method of evaluating valuable information on the membrane surface, such as signal induction, virus infection, and morphological changes of the cell membrane (endocytosis/exocytosi), has recently been presented using new techniques.[1] Currently, the idea that membrane-protein interactions trigger membrane-related phenomena has become mainstream in research on cell membranes.[2,3] Many researchers have previously investigated the structure and functions of (membrane) proteins related to these phenomena.[2,3] The significance of the role of the cell membrane, including the phospholipid bilayer, has gradually been recognized.[4] It is therefore important and necessary to design and develop an on-line detection system for membrane-protein interactions to quantify the function of the cell membrane.

A liposome is composed of a closed bilayer phospholipid membrane that has previously been used as a model cell membrane. Since an immobilization technique was developed by Lundahl and Yang,[5] liposomes have been used as sensor elements in various monitoring methods, such as surface plasmon resonance (SPR),[6] immobilized liposome chromatography (ILC),[7–9] quartz crystal microbalance analysis (QCM)[10] and dielectric dispersion analysis (DDA).[11,12] It is a common feature of these methods that the liposomes are immobilized as sensor elements on the detector surface or gel support and that the liposome-protein interaction can be directly evaluated. In general, the detection principal is based on the adsorption of protein on the liposomal surface or the retardation of elution behavior resulting from the interaction between liposomes and proteins.[6–12] A liposome entrapping calcein has recently been developed to improve the sensitivity of ILC.[13] It is suggested that calcein release is a useful index for the detection of the protein-liposome interaction because the release of calcein is affected by membrane characteristics such as membrane fluidity and permeability. An electrolyte-entrapped immobilized-liposome electrode (ILE) has recently been developed and applied to the analysis of the protein-lipid membrane interaction using amperometry.[14,15] These methods are based on the release of detectable materials entrapped in an immobilized liposome. Although there have been many reports on this issue, a common mechanism of release has not been presented because of the lack of fundamental knowledge about the relationship between the membrane properties and the release behavior.

The purpose of this study is to obtain fundamental data on the release of detectable materials from immobilized liposomes to design a liposome-based stress sensor effectively. Small fluorescent molecular calcein can be used as a detectable material because calcein becomes entrapped inside liposome during high-concentration quenches. We first investigated calcein release from liposomes in the presence of proteins at various pHs. We also investigated the protein-liposome interaction using immobilized liposomes for comparison with the above results. The effects of lipid composition and protein type on calcein release were also studied. On the basis of these results, a possible model for calcein release due to protein-membrane interaction under the stress condition is presented.

2. Materials and Methods

2.1 *Materials*

The phospholipids used were 1-palmitoyl-2-oleoyl-*sn*-glycero-3-phosphocholine (POPC), 1,2-dioleoyl-*sn*-glycero-3-phosphocholine (DOPC), 1,2-dipalmitoyl-*sn*-glycero-3-phosphocholine (DPPC), and 1,2-dimirystoyl-*sn*-glycero-3-phosphocholine (DMPC) (Avanti Polar Lipids (Birmingham, England, UK). Poly(ethylene glycol) (PEG1540, 4000 and 6000, MW=1 k, 3 k, and 6 kD) and dextran (Dex)100 k-200 k (MW=100k-200 kDa) were purchased from Wako Pure Chemicals Ltd. (Osaka, Japan). 1-Anilinonaphthalene-8-sulfonic acid (ANS) and 1,6-diphenyl-1,3,5-hexatriene (DPH) were purchased from Molecular Probes (Junction City, OR, USA). Calcein was purchased from Dojindo (Kumamoto, Japan). The nonionic detergents Triton X-100 and X-405 were purchased from Sigma (New York, NY, USA). Salts and other chemicals of analytical grade were purchased from Wako Pure Chemicals Ltd.

2.2 *Preparation of liposomes*

Phospholipid in chloroform (10 mg/ml) was dried in a round-bottom flask by rotary evaporation. The lipids were redissolved in diethylether twice and then evaporated to form a dry lipid film. The lipid film was kept under vacuum for at least 3 h and then hydrated by being dispersed in buffer T (50 mM Tris-HCl buffer, pH 7.5, 150 mM NaCl) or 100 mM calcein solution to form multilamellar liposomes (MLVs). For the preparation of unilamellar liposomes by extrusion, the MLV suspension was frozen in dry ice/ethanol (–80°C) for five cycles, and passed 15 times through two stacked polycarbonate filters with 100-nm pores (Nuclepore, Costar, Cambridge, MA) at room temperature by using an extrusion device (Liposofast; Avestin Inc.). To prepare liposomes entrapping calcein, free calcein was removed by gel permeation chromatography (Sepharose 4B, ϕ 15 mm, height 200 mm). A commercial kit from Wako Pure Chemicals Ltd. was used to determine the lipid concentration.

2.3 *Calcein release assay*

For the calcein release experiments, 10 μl of a solution of liposomes entrapping calcein was added to buffer T with and without CAB (final concentration 10 μM) at various pHs, and 25 μl of a solution of the liposomes was added to a final concentration of 0.1 mM phospholipid (Scheme 1). At pH4 or 5, a citrate buffer containing 150 mM of NaCl was used. The release fraction (RF) of calcein was calculated from its fluorescence intensity (excitation wave length: 490 nm, emission wave length: 520 nm) as

$$RF = 100(I(t) - I_c) / (I_{total} - I_c)\ (\%), \tag{1}$$

where $I(t)$ is the intensity at time t, and I_c and I_{total} are the intensities immediately after the start of the release analysis and immediately after the addition of Triton X-100, respectively. First-order kinetics were employed to analyze calcein release

$$RF = RF_{max}(1-\exp(-k_{per}t)), \tag{2}$$

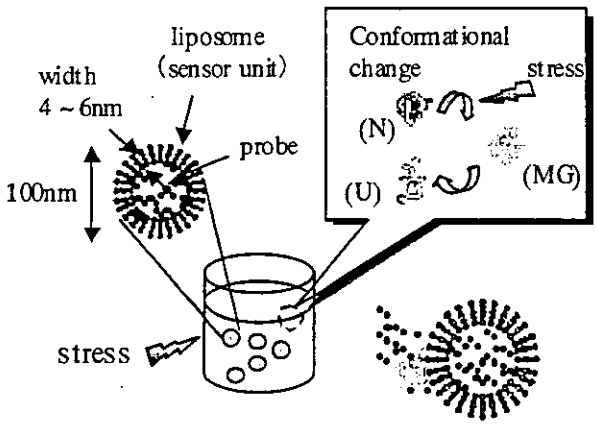

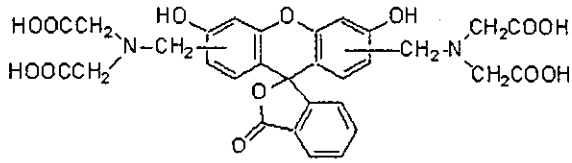

Chemical structure of calcein used as probe.

Scheme 1. Experimental system used in this study and chemical structure of calcein. Symbols are; N: native state; MG: molten-globule state; U: unfolded state.

where RF_{max} and k_{pert} represent the maximum value of RF and the release rate constant, respectively. To determine RF_{max}, all experiments were run until the value of calcein fluorescence reached a constant value.

2.4 *Measurement of local hydrophobicity*

The local hydrophobicity (*LH*) of the proteins was analyzed using an aqueous two-phase partitioning method.[7–9,16] When the pH is set at the pI under low ionic strength conditions, the partition coefficients of the proteins depend mainly on the hydrophobic effect. When Triton X-405 is added to the PEG/Dex system, Triton X-405 partitions preferably to the top (PEG) phase. The protein that binds hydrophobically with Triton X-405 is likely to be partitioned to the top phase. The difference between the partition coefficients of the proteins in two-phase systems with and without 1 mM Triton X-405 gives the *LH* of the proteins. The *LH* of the proteins was defined as

$$LH = \ln K_{with\ ligand} - \ln K_{without\ ligand} \tag{3}$$

where $K_{with\ ligand}$ and $K_{without\ ligand}$ are the partition coefficients of the proteins in the aqueous two-phase systems with and without 1 mM Triton X-405, respectively.

2.5 *Membrane properties of liposomes*

The membrane fluidity of the liposomes was determined from fluorescence polarization (P) by measuring the fluorescent intensity of 1,6-diphenyl-1,3,5-hexatriene (DPH) according to the method of Lentz.[17] The fluorescence probes were partitioned into the lipid bilayer in the following way. The solution of DPH (in ethanol) was added to the liposome suspension to maintain the lipid/probe molar ratio at 250($[DPH]_{final}$=2 μM). The mixture was then incubated for at least 1 h at room temperature with gentle stirring. The amount of probe remaining in the outer aqueous phase of the liposomes was negligible because they show little fluorescence in water. The fluorescence intensity of samples was measured with a spectrofluorometer to which excitation and analyzing polarizers (FP-777 JASCO Co.Ltd., Japan) were attached. The sample was excited with vertically polarized light (360 nm) and then the emission intensity at 430 nm both parallel ($I_{//}$) and perpendicular ($I_{\perp}$) to the excited light was recorded. The P of TMA-DPH was calculated using the following equation.

$$P = (I_{//} - I_{\perp}) / (I_{//} + I_{\perp}) \tag{4}$$

The reciprocal value of polarization ($1/P$) was defined as the membrane fluidity. Because DPH is preferably partitioned in the hydrophobic acyl region, $(1/P)_{DPH}$ is considered to be the membrane fluidity of the interior of the liposome membrane.

As for determining the *LH* of the liposomes, the hydrophobic fluorescence probe ANS was used instead of the hydrophobic probe Triton X-405 because according to a previous study[7] the Triton X-405 probe affects the bilayer structure of liposomes. In brief, 20 μl of 1 mM ANS was added to the liposome suspension ([lipid] = 0.25 mM). The fluorescence of the sample solution (I_{ANS}) was measured at an excitation wavelength of 400 nm and an emission wavelength of 470 nm. The relative I_{ANS} was calculated by selecting the I_{ANS} for a liposome (50 nm in diameter) as the unit *LH* of a liposome, LH_{lip} =1. The LH_{lip} of liposomes has been confirmed to correspond to the membrane fluidity of the liposome surface as evaluated using a positively charged hydrophobic probe (trimethylammonium-DPH) (data not shown). In this study, only zwitterionic liposomes were used because charge repulsion between negatively charged ANS molecules and charged lipids may occur.

2.6 *Immobilized liposome chromatography*

An immobilized liposome gel matrix was prepared as previously reported.[7–9] In brief, liposomes were immobilized in a gel matrix (TSKG6000PW; Tosoh Corp., Tokyo) using a covalent-binding method. The amount of immobilized liposomes was determined using a phosphate determination kit (Phospholipid Test Wako Kit; Wako). The immobilized liposome gel was packed in a glass column 5.5×0.5 cm (HR5/5; Amersham Biosciences, Sweden), which was connected to an HPLC (AKTA Purifier; Amersham Biosciences, Sweden). The running buffer (pH 2–7.5) was preincubated in a water bath at 25°C. The retardation of proteins on the immobilization column was expressed as the capacity factor, k_s, which is defined as $k_s = (V_s - V_N) / M_{lip}$, as described by Yoshimoto *et al.*[7] The term V_s is the retention volume of proteins (ml) and V_N is the elution volume of proteins (ml), neither

of which was retarded on the column as determined using native proteins in the absence of stress. The term M_{lip} is the apparent amount of immobilized liposomes (mmol).

3. Results and Discussion

3.1 *Calcein release in the presence of proteins at various pHs*

It is well known that calcein can permeate a phospholipid membrane by controlling its membrane fluidity. Calcein release from POPC liposomes, *RF*, was kinetically analyzed in the presence of CAB at various pHs (Fig. 1(a)). At pH4, a significant release of calcein was observed compared with that released at other pHs. The data obtained under various conditions were fitted using eq. (2) and matched a calculated curve well for time intervals of up to 10 min. The parameters obtained were the release rate constant k_{pert} and the maximum release fraction of calcein RF_{max}. Both parameters (k_{pert} and RF_{max}) reached a maximum at around pH4. The RF_{max} values appear to be proportional to the protein concentration and inversely proportional to the lipid concentration (data not shown). When the RF_{max} values were plotted against the protein/lipid ratio (Φ_c) using a double-logarithmic scale, plots identical to Hill plots could be obtained,[18] as shown in Fig. 1(b). The RF_{max} values were found to depend on Φ_c. The Hill coefficients (the slope of the linear part of the curves at low Φ_c) were 1.1 and 1.2 in the cases of pH 5 and 4, respectively. These values are reasonably close to 1, suggesting that the surroundings of the CAB-lipid binding sites correspond with the permeation sites and that there is no cooperativity between CAB and calcein. According to Butko *et al.*,[18] it is not individual molecules of δ-endotoxin CytA, but their aggregates (with Hill coefficient close to 1) that induce the breakdown of the permeable membrane barrier. Their results are not consistent with our results in spite of

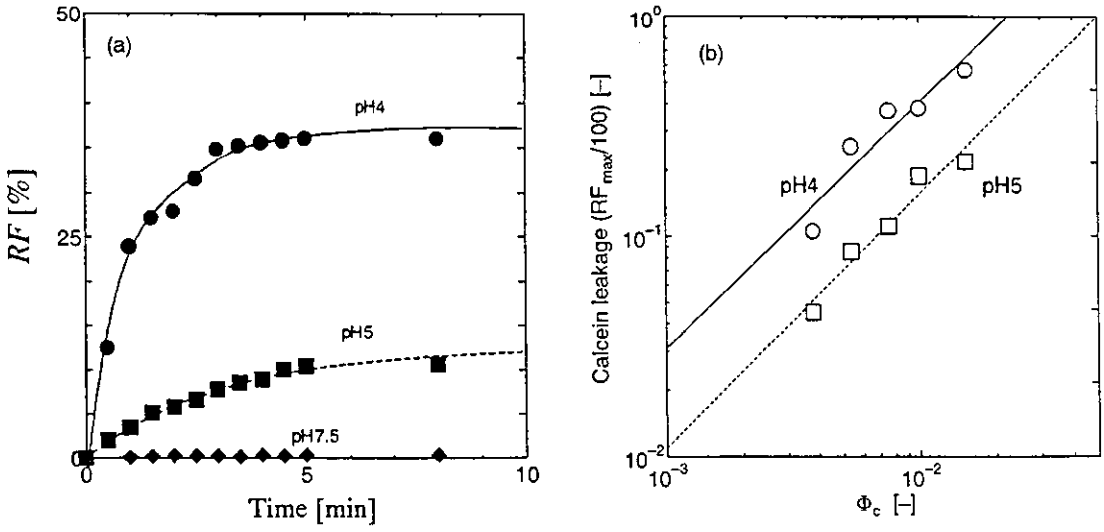

Fig. 1. (a) Time-course of calcein leakage (*RF*) from POPC liposomes in the presence of CAB at various pHs at 25°C. (b) The relationship between the maximum value of RF and the protein-to-lipid molar ratio (G_c).